GeoVirtual 2020 September 14-16 Resilience and Innovation

PERFORMANCE-BASED SEISMIC ANALYSIS OF EMBANKMENTS WITH DSM GRID-TYPE FOUNDATION IMPROVEMENT

Bogart Mendez, Vicki Nguyen & Sachin Patel
Klohn Crippen Berger, Calgary, AB, Canada

ABSTRACT
A performance-based methodology focused on the seismic performance of a structure supported by improved ground based on Deep Soil Mixing (DSM) grids is proposed in this paper. Under a performance-based approach, the design of the DSM grid is conducted such that the target performance of the superstructure is achieved, thus not necessarily imposing the no-liquefaction condition on the enclosed soil within the DSM grid. This concept is explored for the case of embankments supported on square DSM grids. Three-dimensional, non-linear numerical analyses are conducted for a generic embankment founded on DSM-improved ground. The variability of the DSM strength on the embankment performance is evaluated for a given grid configuration. Conclusions and recommendations for this type of analysis are provided.

RÉSUMÉ
Une méthodologie basée sur les performances et centrée sur les performances sismiques d'une structure supportée par un sol amélioré basé sur des grilles du mélange profond des sols (DSM) est proposée dans cet article. Selon une approche basée sur les performances, la conception de la grille DSM est réalisée de telle sorte que la performance objective de la superstructure soit atteinte, n'imposant donc pas nécessairement la condition de non-liquéfaction sur le sol fermé à l'intérieur de la grille DSM. Ce concept est exploré pour le cas de remblais supportés sur des grilles DSM carrées. Des analyses numériques non linéaires en trois dimensions sont effectuées pour un remblai générique fondé sur un sol amélioré par DSM. La variabilité de la résistance du DSM sur les performances du remblai est évaluée pour une configuration de grille donnée. Des conclusions et des recommandations pour ce type d'analyse sont proposées.

1 DSM GRIDS FOR LIQUEFACTION MITIGATION

Deep Soil Mixing (DSM) is a common ground improvement technique used for mitigation of seismic liquefaction. The method consists of installing adjacent columns of DSM in the ground to form walls in a grid arrangement to contain in-situ liquefiable soils. The seismic performance of the DSM-treated ground is improved in the following way (Nguyen et al. 2013): (1) reducing the shear strains imposed on the enclosed soil (the stiffer DSM walls attract shear stresses), thereby reducing the excess pore water pressures generated; (2) providing resistance against lateral deformations and/or vertical settlements even if liquefaction is triggered in the enclosed soils; and (3) providing a barrier against high excess pore pressures migration. A schematic plan view of an idealized DSM grid is shown on Figure 1.

The most significant parameters controlling the effectiveness of the DSM ground treatment are the area replacement ratio, A_r, and the stiffness of the DSM material (Nguyen et al. 2013). The area replacement ratio is defined as the amount (percentage) of soil replaced by the DSM walls, a_{DSM}, to the total area of soil in a unit cell of size S (refer to Figure 1):

$$A_r = \frac{a_{DSM}}{S^2} \quad [1]$$

For a DSM grid composed of single column elements of diameter d, the area of the DSM walls can be computed as a function of the individual column diameter, spacing, S, and overlapping distance, ***e***, as per equations 2 through 6 below, where *N* is the number of DSM columns in each row and β is the chord angle of the overlapping region between columns (Figure 1).

$$a_{DSM} = 0.5\pi d^2(N-1) - 2(N-2)a_{0v} + 4\Delta a \quad [2]$$

$$N = \frac{S}{d-e} \quad [3]$$

$$\Delta a = 0.25(0.25\pi d^2) - a_{0v} \quad [4]$$

$$a_{0v} = 0.25d^2(\beta - \sin\beta) \quad [5]$$

$$\beta = 2\cos^{-1}\left(1 - \frac{e}{d}\right) \quad [6]$$

The equivalent thickness of the DSM walls, d_{eq}, is computed as follows:

$$d_{eq} = S\left(1 - \sqrt{1 - A_r}\right) \quad [7]$$

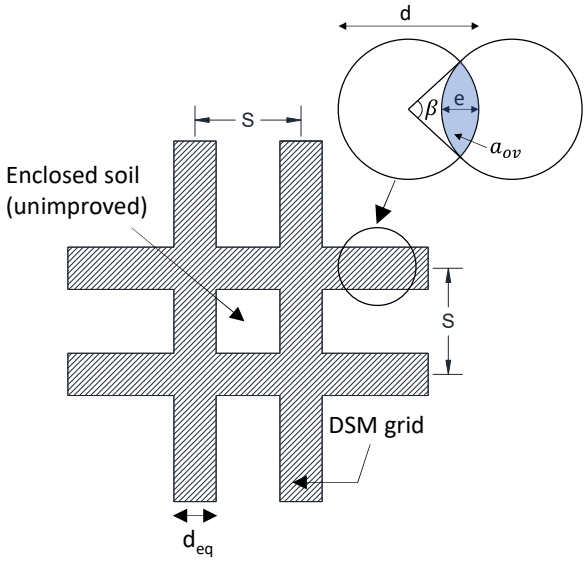

Figure 1. DSM grid unit cell

1.1 Design Methods for DSM Grids

The design methodologies of DSM grids for liquefaction mitigation have evolved from the initial assumption of shear strain compatibility between the DSM walls and the enclosed soils, to methods based on the results of numerical analyses of typical cases (NZGS 2017). Numerical studies (e.g., Nguyen et al. 2012) and experimental results (e.g., Rayamajhi et al. 2015) have shown that the assumption of strain compatibility may greatly overestimate the reduction in shear strain in the soil between reinforcement elements. These results led to the development of the design method of Nguyen et al. (2013) for DSM grids to mitigate liquefaction. The method considers the area replacement ratio and stiffness of the DSM walls to compute the shear stress reduction in the enclosed soil. The effectiveness of the DSM to prevent liquefaction is measured using the factor of safety against liquefaction, FS_{Liq}, obtained using the theoretical framework from Seed and Idriss' simplified procedure (1971). Using the methodology of Nguyen et al., a DSM grid can be designed for a target value of FS_{Liq}, which is typically selected to be at least 1.0. However, this method is only for free field conditions, thus, the seismic performance of a superstructure supported by a DSM grid is not considered in the simplified design methodology. For the case of embankments supported on DSM grids, a numerical analysis that considers site specific information would be more adequate, such that the ground improvement can be designed taking into account the dynamic interaction between the ground improvement and the embankment. A design approach of this type would allow an evaluation of the effectiveness of the ground improvement in terms of the enhancement in the seismic performance of the embankment. An analysis of this type aligns with the philosophy of a performance-based approach, as described next.

2 PERFORMANCE-BASED APPROACH

The focus of a performance-based design is to achieve a target performance in the structure under consideration. In geotechnical earthquake engineering, the performance criteria are specified in terms of engineering parameters that characterize the seismic response of a geotechnical structure, as well as the induced damage (Lubkowski 2019). The consequences of failure and the type of analysis methods are also considered in the selection of the performance criteria.

For the case of geotechnical structures, Lubkowski (2019) proposes a general approach to performance-based design: 1) select suitable performance criteria; 2) develop preliminary design; 3) conduct a performance check, which can be simple if there is no brittle failure mechanism (e.g., liquefaction, slope failure, etc.), or detailed otherwise; 4) consider remedial measures, if required; 5) confirm design solution.

The approach proposed by Lubkowski (2019) is well suited to be applied to the case of dams founded on liquefiable soils with ground improvement treatments, such that a cost-effective solution is obtained. This idea is supported by the experimental results from Adalier and Sharp (2004), who conducted centrifuge testing of an embankment on liquefiable ground. Their experiments included unimproved and improved grounds, where they varied the thickness of the densification zone. Their results for the specific group of tests suggested that *"there may be an optimum depth of densification treatment beneath an earth dam beyond which the reduction of the earthquake-induced deformations is relatively minor".* Based on these results, Adalier and Sharp (2004) suggest that the design of remedial measures should be based on displacement criteria rather than on the factor of safety against liquefaction. This is in line with Finn (2018), who describes this type of situation as one of the most challenging areas of performance-based design, due not only to the difficulties in the selection of the performance criteria, but also in the reliability of the analyses and in the lack of field response data in large dams to allow the assessment of the analysis methodologies.

For the specific problem of an embankment supported on a DSM-grid for liquefaction mitigation, the performance criteria could be based on the seismic deformation of the slopes in the embankment, provided that they are not prone to liquefaction. Under these conditions, a rational, cost-effective design of the DSM grid could be developed by allowing some liquefaction in the enclosed soils, as long as the deformation criteria in the embankment is satisfied for both the operational

basis earthquake (OBE) and the maximum design earthquake (MDE).

Similar concepts have been adopted for building structures founded on DSM grids. For example, Namikawa et al. (2007) conducted 3D Finite Element analyses of a DSM grid case and pointed out that DSM grids can be designed more rationally using a performance-based approach in which a partial damage of the DSM walls could be accepted under the required performance. Yamashita et al. (2018) arrive at similar conclusions based on the results of a seismic response analysis of a piled raft foundation combined with a DSM grid supporting a 12-story base-isolated building under strong earthquake loading. They suggest that the DSM grid could be designed more rationally by following a performance-based approach where minor damage to the DSM walls can be tolerated under strong earthquakes, provided that the required foundation performance is satisfied.

A hypothetical case is presented in this paper to illustrate a performance-based approach for the case of an embankment founded on a DSM grid in liquefiable soil.

3 HYPOTHETICAL CASE OF ANALYSIS

The hypothetical case of a 20 m high embankment founded on liquefiable soil is presented herein. The purpose of the analysis is to illustrate the general process of the performance-based approach for the design of a DSM grid. The analysis considers two levels of ground motions for the design of the ground improvement: an operational basis earthquake (OBE) and the maximum design earthquake (MDE). The embankment cross section is depicted on Figure 2.

The analysis was conducted with the finite difference method using the software FLAC3D 7.0 (Itasca 2019). A three-dimensional model was used to explicitly account for the geometry of the DSM grid in the analysis. The general view of the model is presented on Figure 3.

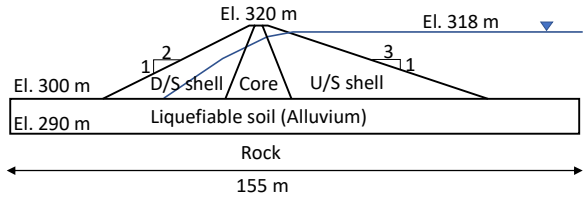

Figure 2. Embankment cross section of analysis case

3.1 Geotechnical Setting and Material Parameters

The case analyzed consists of a rock valley with a 10 m thick, medium dense alluvial deposit at its bottom. The geotechnical profile of the alluvium soil overlying the bedrock is shown on Figure 4 in terms of SPT blow count (a), fines content (b) and shear wave velocities (c). The constitutive model used for each material, as well as the density, ρ, and strength properties are included in Table 1. The elastic properties of the materials are shown in Table 2.

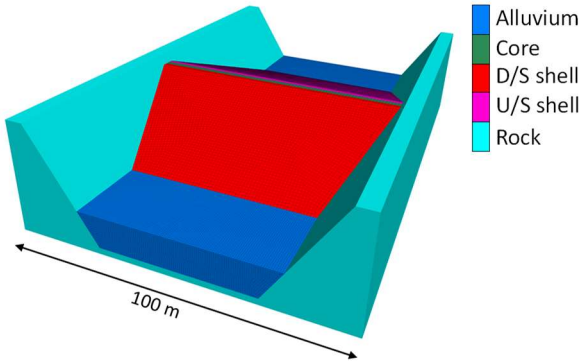

Figure 3. Geometry of the hypothetical embankment

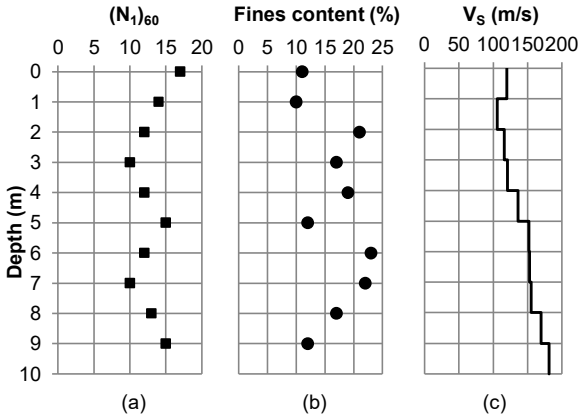

Figure 4. Geotechnical profile of the alluvium soil

Table 1. Material density and strength properties

Material	Model	ρ (kg/m^3)	ϕ_0' (deg)	$\Delta\phi_0$' (deg)	c (kPa)
Alluvium	MC*	1900	30	0	-
Rock	Elastic	2200	-	-	-
Core	MC	2100	5	0	50
D/S shell	MC	2100	37	8	5
U/S shell	MC	2100	34	8	5

* Switched to Finn-Byrne model for dynamic loading. The friction angle of 30° corresponds to the large-strain value.

Table 2. Dynamic material properties

Material	V_{S1} (m/s)	ν	G_{max} (MPa)	G/G_{max} curve
Alluvium	*	0.30	$\rho(V_s)^2$	Seed & Idriss (1970)
Rock	800**	0.30	1408	Silva et al. (2000)
Core	170	0.45	$\rho(V_s)^2$	Vucetic & Dobry (1991)
D/S shell	200	0.30	$\rho(V_s)^2$	Darandeli (2001)
U/S shell	185	0.30	$\rho(V_s)^2$	Darandeli (2001)

* Vs value for each layer as listed on Figure 4c
** Constant value

The friction angle of the downstream (D/S) and upstream (U/S) shell materials is stress-dependent, as per equation [8]. The shear wave velocity of the embankment materials varies with stress as indicated in equation [9]. The atmospheric pressure in equations [8] and [9], P_a, is taken as 100 kPa. The large strain (static) shear modulus of the materials is taken as 30% of the small strain value (G_{max}).

$$\phi' = \phi'_0 - \Delta\phi'_0 \log\left(\frac{\sigma'_v}{P_a}\right) \quad [8]$$

$$V_S = V_{S1}\left(\frac{P_a}{\sigma'_v}\right)^{-0.25} \quad [9]$$

The G/G_{max} degradation curves listed in Table 2 consider the mean curve for the Seed and Idriss model, the curve for a PI = 30 in the Vucetic and Dobry model, the curve for +20 ft depth rock in the Silva et al. model and PI = 15, σ'_0 = 100 kPa for the Darandeli model.

3.2 Ground Motions

The Loma Prieta earthquake recorded at a rock site was used for the example analysis (RSN 788, PEER 2020). The record was scaled to a PGA of 0.13 g for OBE and 0.27 g for MDE ground motions.

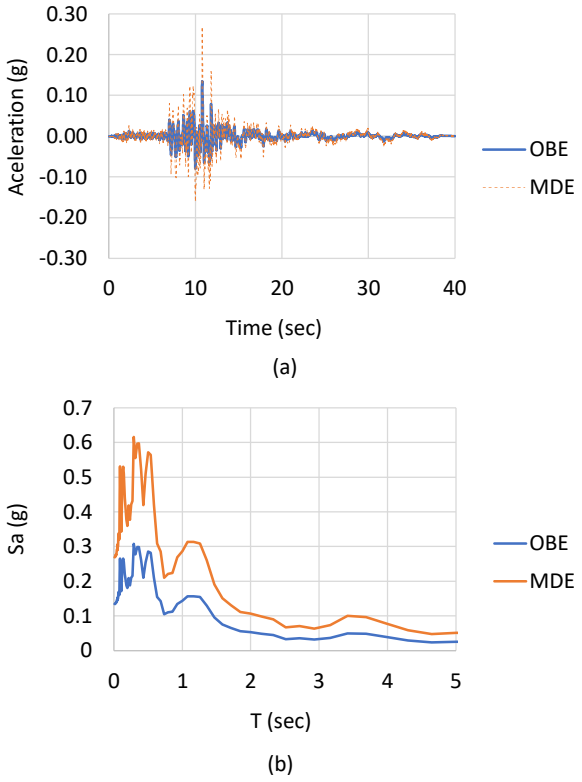

Figure 5. Ground motions considered in the analysis

3.3 Free-field Site Response

The free-field site response of the alluvium layer was evaluated using the 1D equivalent linear methodology as implemented in STRATA (Kottke and Rathje. 2008) for both OBE and MDE ground motions. The PGA values at the ground surface were computed as 0.20 g and 0.34 g for the OBE and MDE cases, respectively. The cyclic stress ratios obtained from the site response analysis were used to compute the factor of safety against liquefaction (FS_{Liq}) using the Seed simplified methodology (Youd et al. 2001). Results are presented on Figure 6(a), where it is noted that for the OBE scenario, liquefaction is only predicted to occur for the lower half of the soil profile.

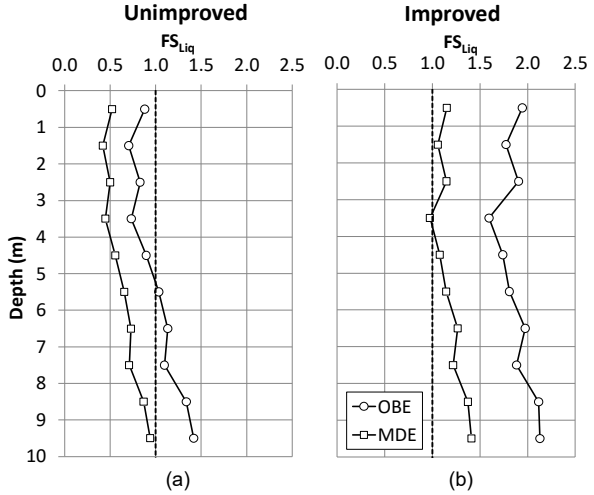

Figure 6. FS_{Liq} for free field conditions; (a) unimproved ground and (b) improved with DSM grid (Ar = 19%). The surface PGA values are 0.20 g and 0.34 g for OBE and MDE, respectively.

3.4 Simplified Evaluation of DSM Grid

The simplified method of Nguyen et al. (2013) was used as a starting point for the preliminary design of the DSM grid. The preliminary design was then included in the 3D numerical model to verify the seismic performance of the soil-grid-embankment system. Equations [1] through [6] were used to compute the area replacement ratio (Ar) for different grid sizes and column diameters of mixed soils and estimate its effectiveness for improving the value of FS_{Liq}. A target Unconfined Compressive Strength (UCS) nominal value of 1 MPa was selected for the DSM material. The shear strength and of the mixed soil was computed as 390 kPa as per the FHWA (2013) guidelines. The stiffness properties of the DSM were estimated using the UCS-Vs correlation proposed by Guimond-Barrett et al. (2013). The properties selected for the DSM are listed in Table 3. The G/G_{max} degradation curve adopted for the DSM material is the model from Silva et al. (2000) for rock, which is considered more appropriate than using a degradation

curve for soils, due to the cementitious characteristics of DSM.

Table 3. DSM properties

UCS (MPa)	ϕ (deg)	c (kPa)	ρ (kg/m^3)	V_S (m/s)	ν	G_{max} (MPa)
1	0	390	1850	550	0.30	560

The FS_{Liq} distribution obtained with the Nguyen et al. (2013) method (for free-field conditions) is shown on Figure 6(b). The target of the preliminary design using Nguyen's method was set as FS_{Liq} of at least 1.0 at all depths for both levels of ground motion. The area replacement ratio that achieves this target is 19%, which can be accommodated with the following grid geometry:

- column diameter: 1.10 m
- grid spacing (S): 10.00 m
- column overlapping (e): 0.28 m
- equivalent wall thickness (d_{eq}): 1.00 m

3.5 Numerical Modelling Procedure

The hypothetical case of analysis was modeled for both the unimproved and improved conditions. For the improved condition, the geometry of the preliminary design was setup in the 3D numerical model to verify the performance of the foundation-embankment system. The mesh size in the model was configurated for wave propagation by using at least 10 elements per wavelength for all materials. The finest mesh size was assigned to the alluvium elements. The frequency content of the ground motions was adjusted to obtain compatibility between the mesh and the time histories selected. The analysis was conducted for undrained conditions.

The analysis sequence considered for the modelling was the following:

- Solve for the initial equilibrium of the alluvium deposit in the rock valley, with the groundwater level at the surface of the alluvium layer.
- For the unimproved model, the next step was to build the embankment. For the improved case, the DSM grid was installed before building the embankment. Five construction stages were simulated for the embankment construction to incrementally build the stress field inside the embankment and the corresponding changes in material strength and stiffness as described in Section 3.1. No construction-induced pore pressures were considered.
- Install the steady-state (long term) pore water pressures in the embankment and solve for static equilibrium. The static factor of safety is computed as a separate model stage for both unimproved and improved conditions.
- Switch the alluvium soil to the Finn-Byrne constitutive model and solve for static equilibrium.
- Invoke the dynamic boundary conditions and apply the seismic load. The dynamic boundary conditions consisted of using a free-field boundary condition on the lateral boundaries of the model, and a quiet boundary at the base of the model. Two different models were used, one for the OBE and another for MDE cases.

The Finn-Byrne constitutive model simulates the dynamic pore pressure generation as a function of the plastic volumetric strain increase, as shown in equation [10]. The model is based on the Mohr-Coulomb constitutive model and it incorporates the Byrne relationship between irrecoverable volume change and cyclic shear strain amplitude to simulate pore pressure generation. The model captures the basic mechanisms that can lead to liquefaction in sand (Itasca 2019).

$$\frac{\Delta\varepsilon_{vd}}{\gamma} = C_1 \exp\left(-C_2 \frac{\varepsilon_{vd}}{\gamma}\right) \qquad [10]$$

Where $\Delta\varepsilon_{vd}$ is the increment of volume strain, ε_{vd} is the accumulated volume strain, γ is the cyclic shear strain, and C_1 and C_2 are the model constants, which can be obtained from laboratory testing or estimated from the SPT blow count (Itasca 2019). For the hypothetical case shown in this paper, the model constants were obtained based on the SPT blow count shown on Figure 4(a) for each depth.

A view of the numerical model including the DSM grid in the alluvium soil is shown on Figure 7.

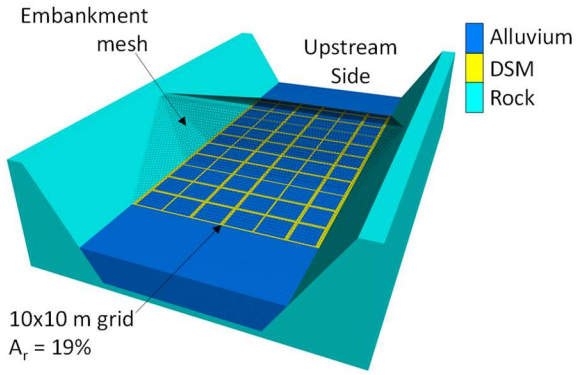

Figure 7. DSM grid in the numerical model for the improved case

3.6 Performance Criteria

The target performance for the hypothetical case analyzed is defined in terms of static factor of safety (FoS) and seismic-induced displacements for the two levels of seismic loading:

- Target static FoS for the long-term condition: 1.5

- Horizontal Deformation for OBE case: 15 cm
- Horizontal Deformation for MDE case: 60 cm
- The available freeboard should be at least 1 m for both seismic cases.

3.7 Model Results: Static Factors of Safety

The static FoS for the long-term condition is shown on Figure 8 below for the cross section through the center of the unimproved and improved models. Results show that the target FoS of 1.5 is not met for the unimproved case. The failure surface develops through the alluvium soil and through the DSM walls in the improved case.

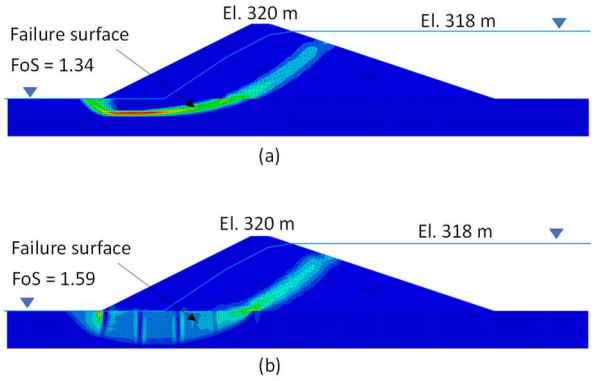

Figure 8. Static FoS for the (a) unimproved and (b) improved cases

3.8 Model Results: Seismic Performance

The seismic response of the unimproved and improved models is presented in this section in terms of deformations and excess pore pressure ratios for both earthquake conditions.

Horizontal deformations for the OBE case are shown on Figure 9(a) and on Figure 10(a) for the MDE case. The horizontal deformations correspond to the center of the downstream slope. The unimproved case developed 24 cm of horizontal deformation. This value diminished to 16 cm for the improved case. This value is slightly larger than the target value of 15 cm set for the OBE case. For the MDE loading, the deformations were computed to be 89 cm and 54 cm for the unimproved and improved cases, respectively. The deformation in the improved case is smaller than the target value of 60 cm for the MDE case.

In terms of the crest settlement, the computed deformations are small compared to the freeboard requirements of at least 1 m for both loading conditions. Crest settlements are presented on Figure 9(b) for the OBE and on Figure 10(b) for the MDE case. Only 15 cm of crest settlement were computed for the MDE in the improved case, which corresponds to a freeboard of 1.85 m. The value computed is small enough to accommodate any reconsolidation settlements that might develop after the end of seismic loading. However, these would be expected to be small because of the DSM grid improvement.

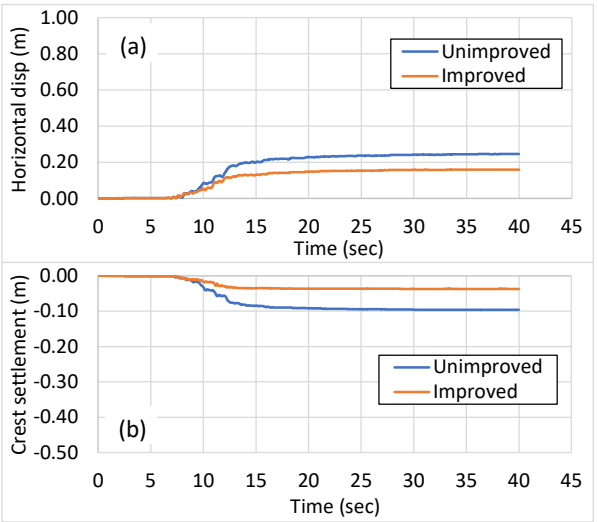

Figure 9. Deformations for the OBE case: (a) horizontal displacements in the DS slope, (b) crest settlement

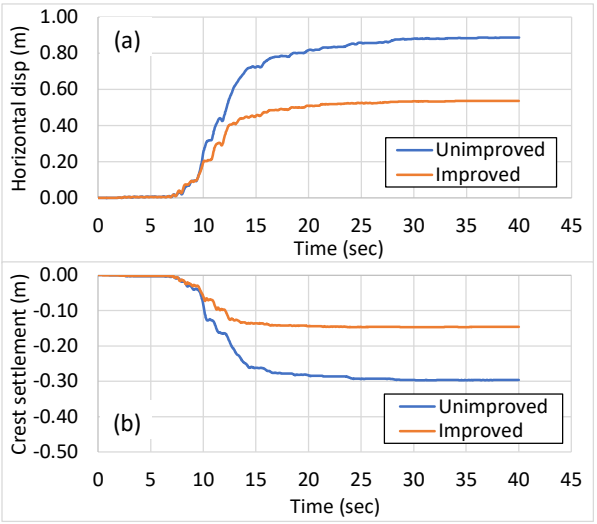

Figure 10. Deformations for the MDE case: (a) horizontal displacements in the DS slope, (b) crest settlement

The seismic-induced pore pressure response is measured in terms of the excess pore pressure ratio, $R_u = \Delta u/\sigma'_{v0}$ (Idriss and Boulanger, 2008). Results are presented for the MDE to illustrate the model response.

The evolution of R_u in the alluvium under the center of the embankment is shown on Figure 11 for the MDE case, where it is observed that the ground improvement reduces the development of excess pore pressure compared to the unimproved case. Also, results show that liquefaction is not triggered in either the unimproved or the improved conditions. This could be attributed to the effect of the increased confinement stress imposed by the embankment, which helps preventing liquefaction

in the soil. Similar results have been observed in experimental results with stone columns under embankments (Tiznado et al. 2019), where liquefaction did not trigger under the center of the embankment where the initial vertical stress was high.

For the toe area on the downstream side, a higher pore pressure response was observed, as noted on Figure 12. This could be attributed, in part, to the initial shear stress in the area under the toe. A similar effect was also observed in the experimental results of Tiznado et al. (2019) and in the numerical analysis of Wang et al. (2015). The upstream toe did not develop liquefaction, likely due to the effect of water pressure on the ground surface on the upstream side.

Interestingly, the results on Figure 12 show that liquefaction triggered at the downstream toe of the embankment for both the unimproved and improved conditions, and even increased for the improved case. This could be explained based on the results of the numerical analysis of Wang et al. (2015), who analyzed the liquefaction potential under a concrete dam and found that for structures with shorter vibration periods, the underlying soil appears to have higher liquefaction potential than the free-field, and the opposite is true for structures with larger vibration periods. Based on these findings, the increase in liquefaction under the toe for the improved case could be explained by the increased stiffness of the improved ground, i.e., a shortening in its vibration period. Therefore, the shortening of the vibration period and the higher initial shear stress at the toe area contribute to the higher liquefaction potential for the improved case over the unimproved case. An overall reduction in the pore pressure response was observed in the remainder of the zones under the embankment, when comparing the improved to the unimproved cases, as observed on Figure 12.

These results show that even when liquefaction is triggered in some parts of the foundation, the overall seismic performance of the embankment can still be satisfactory. This supports the idea of a performance-based design as opposed to a design focused only on the factor of safety against liquefaction. If the no-liquefaction criteria was the target of this analysis, results show that the proposed DSM grid would not satisfy the design criteria.

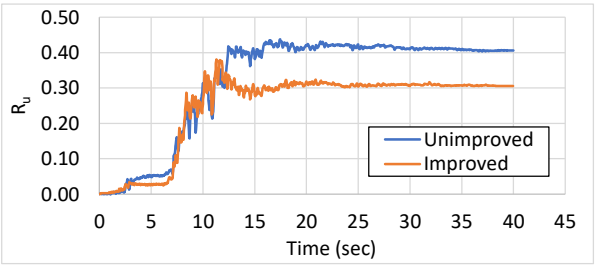

Figure 11. Excess pore pressure ratio in the alluvium under the center of the embankment for the MDE case

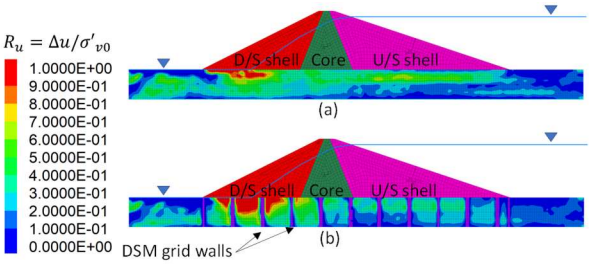

Figure 12. Excess pore pressure ratio for the MDE case: (a) unimproved, (b) improved

3.9 Variability of the DSM Strength

The variability in the DSM strength can have an important effect on the performance of the embankment-foundation system, especially because the construction techniques of the DSM can render large coefficients of variations (COV) in its properties. To illustrate the potential effects of strength variability, Figure 13 shows a hypothetical strength distribution of UCS for different coefficients of variation. A log-normal probability distribution was used to generate three scenarios with the same average value of UCS = 1 MPa but with coefficients of variation of 0.4, 0.5 and 0.6. The strength distribution shows that the strengths skew towards lower values when the COV increases. To evaluate the impact on the response of the hypothetical embankment presented in this paper, the static FoS was computed for the case of a random strength distribution in the DSM with COV = 0.40. The computed FoS for this case reduced from 1.59 for the deterministic case (constant UCS = 1 MPa) to 1.55. The effect in terms of seismic deformations was not evaluated due to lack of time for preparing this paper. However, it is expected to have an impact in the final deformations. The variability in strength should be considered for DSM projects, as it is a known condition and an important factor influencing the results.

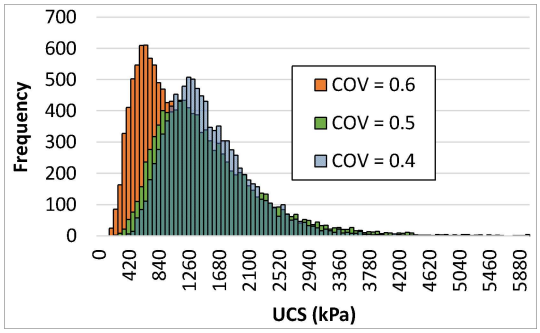

Figure 13. Variability on the DSM compressive strength

4 CONCLUDING REMARKS

The hypothetical case of an embankment founded on liquefiable soils improved with a DSM grid was presented to illustrate how a performance-based design

philosophy can be applied to these types of scenarios. The results of the numerical analysis showed that even when liquefaction triggered in some areas of the foundation soils, the seismic-induced deformations met the design criteria, thus achieving a rational design that considers the dynamic interaction of the embankment-foundation system.

ACKNOWLEDGMENTS

The authors would like to thank Klohn Crippen Berger for the sponsorship received for the preparation of this document.

5 REFERENCES

Adalier, K., Sharp, M.K. 2004. Dynamic Behavior of Embankment Dam on Liquefiable Foundation Subject to Moderate Earthquake Loading. *13th World Conference on Earthquake Engineering*, Vancouver, B.C., Canada August 1-6, Paper No. 1025.

Byrne, P. 1991. A cyclic shear-volume coupling and pore-pressure model for sand. *Proceedings of the 2nd international conference on recent advances in geotechnical earthquake engineering and soil dynamics*. Vol. 1: 47-55. St. Louis, USA.

Darendeli, M. (2001). Development of a New Family of Normalized Modulus Reduction and Material Damping Curves, *Ph.D. Dissertation*, University of Texas.

FHWA 2013. Deep Mixing for Embankment and Foundation Support, Design Manual. *Federal Highway Administration*, Publication No. FWHA-HRT-13-046.

Finn, L.W.D. 2018. Performance Based Design in Geotechnical Earthquake Engineering. *Soil Dynamics and Earthquake Engineering*, vol. 114: 326-332.

Guimond-Barrett A., Nauleau E., Le Kouby A., Pantet A., Reiffsteck P., and Martineau F. 2013. Free-Free Resonance Testing of In situ Deep Mixed Soils. *Geotechnical Testing Journal*, 36(2): 283-291.

Idriss, I. M., and Boulanger, R. W. 2008. Soil liquefaction during earthquakes. Monograph MNO-12, EERI.

Itasca 2019. Fast Lagrangian Analysis of Continua in 3D (FLAC3D), version 7.0.

Kottke, Albert R., and Ellen M. Rathje. 2008. Technical manual for Strata. *Report No.: 2008/10*. Pacific Earthquake Engineering Research Center, University of California, Berkeley.

Lubkowski, Z. 2019. Performance-Based Geotechnical Earthquake Engineering – How Can We Use it in Practice? *SECED 2019 Conference*, Society for Earthquake and Civil Engineering Dynamics, Greenwich, London.

Namikawa et al. 2007. Finite element analysis of lattice-shaped ground improvement by cement-mixing for liquefaction mitigation, *Soils and Foundations*, vol. 47(3), 559-576.

Nguyen, T.V., Rayamajhi, D., Boulanger, R.W., Ashford, S.A., Lu J., Elgamal, A., and Shao, L. 2012. Effect of DSM Grids on Shear Stress Distribution in Liquefiable Soil. *Geocongress 2012*, ASCE: 1948-1957.

Nguyen, T.V., Rayamajhi, D., Boulanger, R.W., Ashford, S.A., Lu J., Elgamal, A., and Shao, L. 2013. Design of DSM Grids for Liquefaction Remediation. *Journal of Geotechnical and Geoenvironmental Engineering*, ASCE, 139(11): 1923-1933.

NZGS 2017. *Earthquake Geotechnical Engineering Practice, Module 5: Ground improvement of soils prone to liquefaction*. New Zealand Geotechnical Society.

PEER 2020. Ground Motion Database, Pacific Earthquake Engineering Research Center. Accessed online during May 2020.

Rayamajhi, D., Tamura, S., Khosravi, M., Boulanger, R.W., Wilson, D.W., Ashford, S.A., and Olgun, C.G. 2015. Dynamic Centrifuge Tests to Evaluate Reinforcing Mechanisms of Soil-Cement Columns in Liquefiable Sand. *Journal of Geotechnical and Geoenvironmental Engineering*, ASCE, 141(6).

Seed, B., and Idriss I.M. 1970. Soil Moduli and Damping Factors for Dynamic Response Analyses, *Earthquake Engineering Research Center*, Report No. EERC 70-10.

Seed, H. B., and Idriss, I. M. 1971. Simplified procedure for evaluating soil liquefaction potential. *Journal of Soil Mechanics and Foundations Division*, 97(9): 1249–1273.

Silva, W. Darragh, R., Gregor, N., Martin, G., Abrahamson, N., and Kircher, C., 2000. Reassessment of Site Coefficients and Near-Fault Factors for Building Code Provisions Program Element: II, 98-HQ-GR-1010, Report to USGS.

Tiznado, J.C., Dashti, S., Wham, B.P., Ledezma, C. 2019. Centrifuge study of the seismic response of embankments on liquefiable soils improved with dense granular columns. *Earthquake Geotechnical Engineering for Protection and Development of Environment and Constructions*. Associazione Geotecnica Italiana, Rome, Italy, ISBN 978-0-367-14328-2.

Vucetic, M., Dobry, R. (1991). Effect of soil plasticity on cyclic response *Journal of Geotechnical Engineering*, ASCE, 117(1): 89-107.

Wang, G., Wei, X., Liu, H. 2015. Liquefaction evaluation of dam foundation soils considering overlying structure. *Journal of Rock Mechanics and Geotechnical Engineering,* Vol. 7: 226 – 232.

Yamashita et al. 2018. Seismic response analysis of piled raft with grid-form deep mixing walls under strong earthquakes with performance-based design concerns, *Soils and Foundations*, vol. 58, 65-84.

Youd, T.L. and Idriss, I.M. 2001. Liquefaction Resistance of Soils: Summary Report from the 1996 NCEER and 1998 NCEER/NSF Workshops on Evaluation of Liquefaction Resistance of Soils. *Journal of geotechnical and Geoenvironmental Engineering*, ASCE, 127(4): 297-313.